ELSEVIER

Contents lists available at ScienceDirect

Journal of Power Sources

journal homepage: www.elsevier.com/locate/jpowsour





Techno-economic analysis of non-aqueous hybrid redox flow batteries

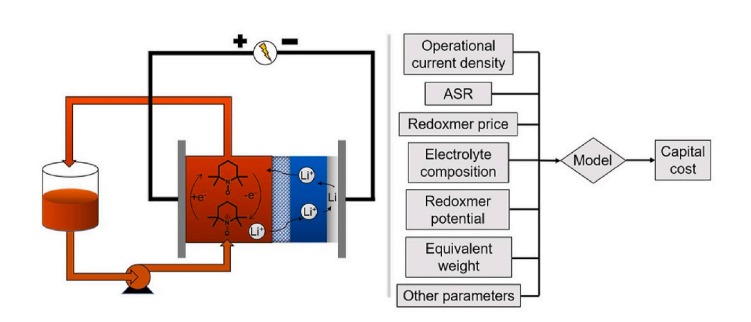
Zhiguang Li ^{a,b,d}, Xiaoting Fang ^{b,d}, Lei Cheng ^{a,c}, Xiaoliang Wei ^{d,**}, Lu Zhang ^{a,b,*}

- ^a Joint Center for Energy Storage Research, Argonne National Laboratory, 9700 South Cass Avenue, Lemont, IL, 60439, USA
- ^b Chemical Sciences and Engineering Division, Argonne National Laboratory, 9700 South Cass Avenue, Lemont, IL, 60439, USA
- ^c Material Sciences Division, Argonne National Laboratory, 9700 South Cass Avenue, Lemont, IL, 60439, USA
- ^d Indiana University-Purdue University Indianapolis, 723 West Michigan Street, Indianapolis, IN, 46202, USA

HIGHLIGHTS

- We established a techno-economic model of non-aqueous hybrid redox flow batteries
- Sensitivity analyses in terms of cycling and material parameters were conducted
- Developing cheap and soluble redxomers remains as the most critical task.
- This framework can evolve for general analysis of various RFB systems.

G R A P H I C A L A B S T R A C T



ARTICLE INFO

Keywords:
Nonaqueous redox flow battery
TEMPO
Techno-economic model
Capital cost
Sensitivity analysis

ABSTRACT

Renewable energy has become indispensable to improving human life, but its growth is hampered by a lack of cost-effective energy storage systems to solve the intermittency problem. Non-aqueous hybrid redox flow batteries (NAqHRFBs), based on lithium metal anode and organic redox molecules (redoxmers), have been investigated as an attractive energy storage option because of their high cell voltages and energy densities compared to other redox flow battery candidates. However, little is known about the economic potential of NAqHRFBs, as well as the operational and materials impacts. This work establishes a techno-economic model to analyze the capital costs of NAqHRFBs with selected organic redoxmers, including 2,2,6,6-tetramethylpiperidine-1-oxyl (TEMPO). Sensitivity analyses for current density, area-specific resistance, cell voltage, electrolyte composition, redoxmer price, and equivalent molecular weight indicate the key factors in controlling NAqHRFB capital cost. To make the current NAqHRFB cost-effective, the first priority is to increase the operation current density over 10 times of those used in lab-scale tests, followed by adjusting redoxmer-related characteristics to afford more cost reduction space such as decreasing the unit price by ~20 fold. The results have shed light on potential material development and system engineering directions to make NAqHRFBs viable for renewable energy storage.

E-mail addresses: xwei18@iupui.edu (X. Wei), luzhang@anl.gov (L. Zhang).

^{*} Corresponding author. Joint Center for Energy Storage Research, Argonne National Laboratory, 9700 South Cass Avenue, Lemont, IL, 60439, USA.

^{**} Corresponding author.

1. Introduction

For a long time, the development and implementation of renewable energy technologies have been of great importance because of their ability not only to help alleviate the greenhouse gas issue by reducing fossil fuel consumption but to protect consumers when fuel prices surge. One of the primary obstacles to broadening the application of renewable energies is the lack of efficient, energy-dense and cost-effective grid storage systems with the design flexibility to handle the intermittency issue. Pumped hydro storage contributed 152 GW-96% of the world's storage capacity—in 2020 due to its extremely low cost, but its use is limited because of its strong reliance on climate and geographical conditions [1]. Redox flow batteries (RFBs), however, possess significant advantages, such as high efficiency, fast response, long life, flexible scalability, and distributed installation, and thus have attracted considerable attention in recent years [2]. Among the various RFB chemistries investigated, the aqueous all-vanadium redox flow battery (VRFB) is the most commercially successful system to date, with a number of megawatt (MW)-scale demo installations around the world [3]. Other RFBs, such as zinc-bromine, all-iron, lead-acid, and, more recently, organic systems, are also rapidly growing [4]. However, wide-spread utilization of RFB technology is impeded by a variety of critical factors including high capital cost, limited energy/power density, and long-term operational stability. For instance, the capital cost for a 4 MWh/1 MW VRFB system, as estimated in a cost model, is as high as \$447 kWh⁻¹, primarily because of the expensive chemical (V₂O₅) used [5]. Thus, there is still a long way to go to meet the near-term and long-term cost targets of \$250 kWh⁻¹ and \$150 kWh⁻¹, respectively, for a storage system providing 4 h of storage set by the U.S. Department of Energy (DOE) [6]. It would be extremely useful if the techno-economic characteristics of an RFB candidate could be identified in its infancy stage, before serious R&D efforts are implemented.

Non-aqueous electrolytes have wider electrochemical windows and can enable higher cell voltages for RFBs than their aqueous counterparts [7,8]. Taking advantage of the extremely low redox potential of Li anode (-3.04 V vs. standard hydrogen electrode), nonaqueous hybrid RFBs (NAqHRFBs) hold great promise to achieve high cell voltage (>3 V) and energy density. The "hybrid" nature of NAqHRFBs is derived from the immobile Li metal anode and the flowing catholyte. The possibility of delivering high energy density gives NAqHRFBs a significant advantage over aqueous and other nonaqueous RFBs. A variety of catholyte redoxmers, including 2,2,6,6-tetramethylpiperidine-1-oxyl (TEMPO) [9], ferrocene [10,11], anthraquinone [12], dialkoxylated benzene [13], and polysulfide [14], have been investigated for NAqHRFBs. Among them, TEMPO has the unique advantages of superior solubility (4-5 M), high redox potential (3.5 V vs. Li/Li⁺), fast redox kinetics, and excellent chemical stability. In our previous work, a Li/TEMPO NAqHRFB using a concentrated TEMPO catholyte (2 M) [9] demonstrated a high discharge energy density of 126 Wh·L⁻¹, which is approximately four times that of VRFB at a comparable vanadium ion concentration [15]. The major drawbacks of NAqHRFBs are closely associated with the Li metal anode-slow deposition/dissolution reactions, Li dendrite growth, coupled energy and power at anode, and air sensitivity—but the recent advances in Li metal anode have demonstrated practical and appealing cycle life and safety features [16,17]. This has made it worthwhile to evaluate the competitiveness of NAqHRFBs in terms of capital cost.

In an early cost analysis by Darling et al., NAqHRFBs were estimated to have the lowest system price among various RFBs under generic, unoptimized conditions [18], illustrating the encouraging attributes of NAqHRFBs. However, this cost model was based loosely on physicochemical and electrochemical property sets that are typical for nonaqueous RFBs, without either identifying a specific catholyte redoxmer or examining the effects of relevant operational and material metrics, such as current density, area-specific resistance (ASR), pump loss, redoxmer price, and so on. These limitations have resulted in missed opportunities to explore the system parameters for further cost

reduction. In addition, despite various cost analyses developed for aqueous RFBs and non-aqueous organic RFBs [19–22], a lack of such studies for NAqHRFBs has hampered the discovery of key cost-determining factors and slowed the development pace of this unique RFB technology.

In this study, we have developed a techno-economic analysis (TEA) model to investigate the system-level performance and cost elements of NAgHRFBs. This model is constructed to include previously underaddressed efficiency loss factors, such as pump loss and heat generation. TEMPO was selected as a model catholyte redoxmer because of its above-stated advantages and established NAqHRFB cell performance, but other redoxmer candidates with different molecular weights, redox potentials and unit prices are also considered as variables in the TEA model. The effects of key operation- and redoxmer-related parameters on the capital cost of NAqHRFBs are evaluated through associated sensitivity analyses. Tailoring these parameters effectively reduces the capital cost of NAqHRFBs to a level competitive with VRFBs and close to DOE's cost target. Our TEA results indicate that the current density, redoxmer price and electrolyte composition are among the most significant cost controllers. The findings suggest future potential research directions towards realization of cost-competitive and high-performance NAgHRFBs.

2. Methods

2.1. NAqHRFB stack components

The schematic of a NAqHRFB multi-cell stack system is shown in Fig. 1. Each single cell in the stack consists of a graphite felt electrode at the catholyte side, a Li-graphite anode, a porous separator, bipolar plates (BPPs) that connect the two adjacent cells in series, and two gaskets for sealing. The Li-graphite anode consists of directly stacked lithium foil and graphite felt to provide improved anode protection. Compared to a Li metal anode, the Li-graphite anode introduces intercalation electrochemistry with graphite felt as the Li⁺ host, instead of the more challenging Li metal deposition/dissolution reaction, to mitigate Li dendrite growth and increase cycle life while still maintaining the same redox potential as Li metal [9,11]. At the ends of the stack are two current collectors and two end plates that bolt all the components together. The NAqHRFB system also includes a pump for circulating the catholyte, a tank that stores the catholyte, a heat exchanger (HEX) that can cool down the reacted catholyte to retain safe working temperatures, and a power conversion system (PCS, not shown in Fig. 1) for DC-AC conversion. Fig. S1 in the Supporting Information shows an exploded view of a single cell. Typical stack parameters are shown in Table S1 in the Supporting Information [23].

2.2. Performance metrics and materials costs

The TEA model for a NAqHRFB system is based on an energy/power scale of 4 MWh/1 MW. The capital cost of an RFB system is closely associated with its practical performance metrics, such as working voltage, current density, and efficiency, which affect the achievable energy capacity and power output. Therefore, it is necessary to first define these metrics with available parameters.

2.2.1. Effective discharge voltage

Given that NAqHRFBs are for energy storage applications, the discharge voltage is used to determine the power output [6]. In addition to the energy loss caused by ASR, the use of a pump and possibly a heat exchanger, as well as shunt current loss, results in efficiency drop. Compared to aqueous electrolytes, nonaqueous electrolytes' characteristics include significantly high viscosity and resistivity. As a result, high pump power and heat generation are expected during the operation of nonaqueous RFBs. In this study, we do not consider the shunt current due to the low electrolyte conductivity. According to a cost analysis, the

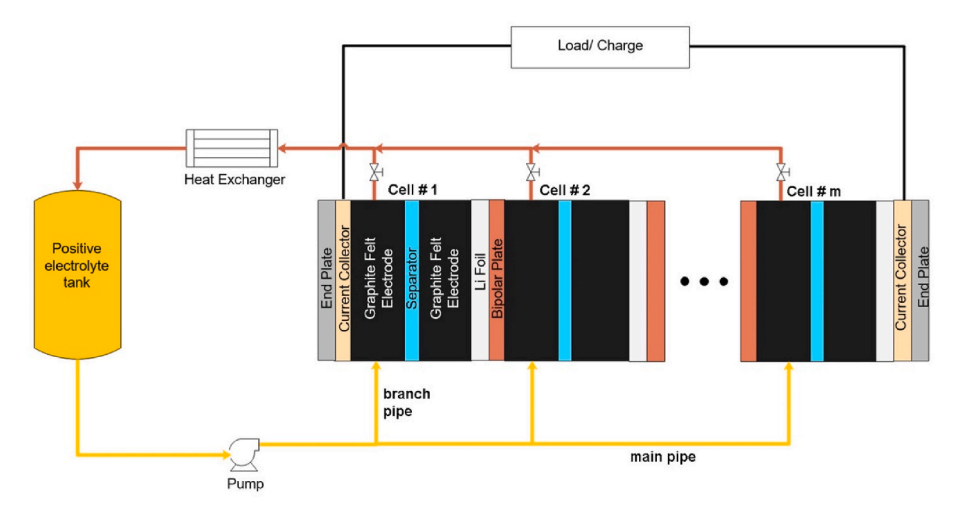


Fig. 1. Schematic diagram of a NAqHRFB multi-cell stack. The cells are series-connected through carbon-stainless steel bipolar plates (BPPs) and are sealed via compression. The arrows indicate catholyte flow direction.

shunt current loss of VRFBs is about 3% on the same 4 MWh/1 MW scale [24]. Since the conductivity of our carbonate electrolyte is about 1% that of the acidic vanadium electrolyte [25], the shunt current loss is expected to be negligible for NAqHRFBs at the same stack voltage. Therefore, in our TEA model, only the energy penalties caused by the ASR, heat exchanger, and pump are considered.

To begin, we introduce a term called the average voltage, V_{avg} , to quantify the practical voltage of a single NAqHRFB cell caused by the ASR-related loss, as shown in Eq. (1):

$$V_{avg} = U - iR \tag{1}$$

where U is the theoretical cell voltage (e.g., 3.5 V for Li/TEMPO battery), i is the current density, and R is the ASR, which includes summative contributions from ohmic (R_{Ω}) , kinetic $(R_{\rm CT})$ and mass transport $(R_{\rm MT})$ losses in the flow cell. Assuming the stack contains m single cells, as shown in Fig. 1, the average discharge voltage of the whole stack is $mV_{\rm avg}$. For a given flow cell test, the ASR can be obtained experimentally by electrochemical impedance spectroscopy (EIS) measurements of the flow cell. The $V_{\rm avg}$ can also be derived from the discharging voltage curve of the flow cell by integrating the instantaneous voltage over the state of charge (SOC) and subsequently dividing the integral by the difference between the initial and the final SOCs [19]. For example, a $V_{\rm avg}$ of 3.09 V was obtained from a Li-graphite/TEMPO flow cell (see Fig. S2a in the Supporting Information for the voltage curve).

A second term, effective discharge voltage, V_{eff} , integrates the loss resulting from pump power consumption in a single flow cell with V_{avg} . Because ASR and pump use are inevitable in NAqHRFB cells, they are included in V_{eff} , but since the heat exchanger is needed only at elevated stack temperature conditions, it is not included in V_{eff} and is analyzed separately in Section 2.4. To estimate the $V_{\rm eff}$, the pump loss is computed based on the pressure drop across a single cell. The pressure drop is divided into two parts: one part caused by electrolyte flowing through the porous graphite felt electrode ($\Delta P_{\rm E}$) and the other part by the electrolyte-pipe friction ($\Delta P_{\rm p}$). While regular RFBs require pumping both electrolytes, an advantage of NAqHRFBs is that only a single electrolyte needs to be pumped, leading to reduced pump and piping loss. These pressure drops are evaluated using Darcy's law, as shown in Eq. (2), and the Hagen-Poiseuille equation, shown in Eq. (3), respectively (see Supporting Note S1 for a discussion of the Reynolds numbers of electrolyte flows in porous electrode and in pipe) [26]:

$$\Delta P_E = \frac{L}{W} \frac{\mu Q}{K t_E} \tag{2}$$

$$\Delta P_p = \frac{128\mu lQ}{\pi D^4} \tag{3}$$

where L, W, and $t_{\rm E}$ are the length, width, and thickness of the porous electrode used in a single cell, K is the permeability of the electrode, μ is the viscosity of the electrolyte, Q is the flow rate, and l and D are the length and inner diameter of the pipe. Typically, the through-electrode pressure drop is significantly higher than the piping pressure drop. Each cell in the stack contributes equally to the overall through-electrode pressure drop. For a NAqHRFB stack containing m single cells, the pump energy consumption ($W_{\rm pump}$) used to overcome pressure drops at each cell can be estimated using Eq. (4):

$$W_{pump} = \frac{(\Delta P_E + \frac{\Delta P_P}{m})Q}{\eta} \tag{4}$$

where η is the pump efficiency. Here, the total piping loss is approximately equally split over the cells in the stack. Based on the results, the $V_{\rm eff}$ of a single cell can be found using Eq. (5):

$$V_{Eff} = V_{avg} \frac{(V_{avg} iA - W_{pump})}{V_{avg} iA} \tag{5}$$

where A is the active electrode area of the cell.

2.2.2. Material and cell metrics

With the effective discharge voltage V_{eff} , the amount of TEMPO (in mole) needed for achieving the nominal energy (E_{d}) can be obtained with Eq. (6):

$$n_{TEMPO} = \frac{E_d}{nV_{eff} F \cdot DOD} \tag{6}$$

where n is the number of electrons involved in the reaction (e.g., n=1 for Li/TEMPO), F is the Faraday constant, and DOD is the depth of discharge retrieved as the ratio of the discharged to theoretical capacities. The DOD value is 60% according to the voltage curve in Fig. S2 in the Supporting Information. The catholyte consists of 2 M TEMPO in 2.3 M lithium hexafluorophosphate (LiPF $_6$) in a solvent mixture of ethylene carbonate(EC), propylene carbonate(PC), and ethyl methyl carbonate (EMC) at 4/1/5 by weight with the presence of 15 wt% fluoroethylene carbonate (FEC) additive [9]. Based on this composition, the amounts of energy components were quantified, and the corresponding amount of Li metal anode was determined.

Power components are also closely associated with the effective discharge voltage $V_{\rm eff}$. Using $V_{\rm eff}$, the actual power output of an

individual stack containing m single cells can be determined with Eq. (7). The power output of an entire NAqHRFB system depends on the configuration of individual stacks. Assuming a storage time of 4 h, the configuration of a NAqHRFB system including N_P parallel strings of N_S series-connected stacks can be determined using Eq. (8):

$$P_{eff} = iAmV_{Eff} \tag{7}$$

$$N_p = \frac{E_d}{4iAmV_{eff}N_s} \tag{8}$$

Based on Eq. (8), the carbon electrode size necessary for achieving the nominal power can be quantified as $N_{\rm P}N_{\rm S}mA$. The total materials cost for energy and power components is obtained by multiplying their quantities by unit prices. The unit prices of most components at the relevant scale have been obtained from various suppliers around the world (see Table 1), except for the bipolar plate (BPP) that will be modeled in the following section.

2.3. BPP model

For NAqHRFB cells, the traditional graphite material is not suitable for use as the anode side enclosure due to possible Li⁺ intercalation reactions. Instead, low-carbon stainless steel demonstrated high electrochemical stability in our previous Li/organic flow cells [9,11]. The catholyte side enclosure still uses traditional graphite materials. Therefore, the BPPs used in NAqHRFB stacks are composed of laminated carbon stainless steel layers. To the best of our knowledge, newly structured BPPs like these are not currently mass-produced. Although certain manufacturers can offer customized BPPs at relatively high costs. it makes good sense to compute the predicted BPP cost at a production volume relevant to the NAqHRFB system. Inspired by Minke's BPP model for fuel cells and RFBs [5], we calculated the BPP cost based on the unit prices of the raw materials used to produce the BPP (see Table 2). The BPPs have the same size as the square graphite felt electrodes, i.e., 0.25 m edge length. The amount of each raw material needed follows an established BPP formulation [23], which is explained in detail in the Supporting Note S2. The investments in manufacturing facilities and processes, including machine and tools, maintenance,

Table 1Cost inputs for the TEA model (See <u>Table S3</u> in the Supporting Information for the suppliers of each component material.).

NAqHRFB Component	Unit Price (USD)
Graphite felt (4 mm thick)	\$75 m ⁻²
Carbon/stainless steel BPP (by computation)	$$3.76 \text{ plate}^{-1}$
Microporous separator	10 m^{-2}
Heat exchanger (HEX)	$$71 \text{ kW}^{-1}$
1" PVC ball valve	$$3.99 \text{ unit}^{-1}$
PVC pipes diameter of 1"	$$1.08 ext{ ft}^{-1}$
PVC pipes diameter of 6"	$$10.81 ext{ ft}^{-1}$
Bolts and nuts	$1.15 \; \mathrm{unit}^{-1}$
UHMW PE gasket	$$76 \text{ m}^{-2}$
Cu current collector	\$90.60 m ⁻²
Al end plat	\$93.43 m ⁻²
PVC frame	$$31 \text{ m}^{-2}$
O ring	$$1.50 \text{ unit}^{-1}$
Pump	$$44 \text{ GPM}^{-1}$
PCS	$$49.60 A^{-1}$
TEMPO	$86 \ kg^{-1}$
Ubiquitous cathodic active material	$$5 \text{ kg}^{-1}$
LiPF ₆	$$20 \text{ kg}^{-1}$
EC	$$1.66 \ { m kg}^{-1}$
PC	$$1.43 \text{ kg}^{-1}$
EMC	$$3.05 \text{ kg}^{-1}$
FEC	$$90.16 \text{ kg}^{-1}$
Li metal	$$13 \text{ kg}^{-1}$
Tank	$$0.75 \text{ gal}^{-1}$
Labor	1 kWh^{-1}
Logistics	$$0.16 \text{ kg}^{-1}$

Table 2Parameters for BPP production model assuming an annual production volume of 192,000 plates [5]. (See raw material suppliers and more details of listed items in Table S2 in the Supporting Information.)

Raw Material		Tooling	
Graphite flake (31 wt% ^a)	$$1.8 \ kg^{-1}$	Investment	\$160,000 [5]
Ketjen black (12 wt% ^a)	$$78.5 \text{ kg}^{-1}$	Cycle time	90 s [5]
Carbon nano-tube (3 wt%a)	$$375 \text{ kg}^{-1}$	Energy	
Chlorinated polyethylene (54 wt% ^a)	\$1.25 kg ⁻¹	Installed capacity	150 kW [5]
Stainless steel	$$0.8 \text{ kg}^{-1}$	Energy cost	0.0648 kWh ⁻¹
Material waste	10%	Other energy	$1 hr^{-1}$
BPP dimensions		Staff	
Width	0.25 m	Labor	$$25 \text{ hr}^{-1}$
Length	0.25 m	Personnel requirement	0.5
Thickness	4 mm	Annual working hour	6000 h
Machine		Annual labor wage	\$75,000
Investment	\$600,000	-	
	[5]		
Depreciation period	8 years		
Interest on initial investment	3%		
Maintenance cost	3%		
Machine utilization	80%		

^a The gravimetric composition at the carbon side of the BPP.

labor, and interest on capital, are also taken into consideration for the BPP cost estimation. The cash flow analysis of the BPP model is shown in Fig. S3. Based on the material and manufacturing costs for producing the needed number of BPPs over an extended period (8 years in this example), the unit price of the BPP is obtained as \$3.76 plate⁻¹, which is then used in the calculation of NAqHRFB capital cost.

2.4. Heat exchanger model

Typically, RFB operation generates heat internally and elevates the electrolyte temperature. Whether a heat exchanger (HEX) is needed depends on the thermal stability of electrolyte. We obtained the decomposition temperatures of TEMPO-based catholyte ingredients—TEMPO, LiPF₆, EC, EMC, PC, and FEC—from literature reports. They are shown in Table S4. The upper temperature limit for the catholyte to avoid decomposition is defined as the lowest thermal stability temperature among these ingredients. Heat generation originates mainly from two sources: the enthalpy change of the redox reaction and the internal resistance of the flow cell. The heat generated from the enthalpy change and the resistive loss are defined in Eq. (9) and Eq. (10), respectively:

$$P_r = \frac{m \cdot i \cdot A \cdot \Delta H_r}{F} \tag{9}$$

$$P_R = i^2 \cdot R_\Omega \cdot m \cdot A \tag{10}$$

where $\Delta H_{\rm r}$ is the enthalpy of reaction.

The thermodynamic properties, including standard enthalpies and specific heat capacities, of the redox species involved (TEMPO, TEMPO⁺, Li, and Li⁺) are not readily available, and experimental testing of them can be labor-intensive. To obtain the enthalpy of the redox reaction, we use density functional theory (DFT) to calculate these thermodynamic parameters, following widely available theoretical methods [27–29]. The thermal enthalpies of the redox species illustrated in Scheme 1 were obtained from DFT with B3LYP function and implemented by Gaussian 16 in Bebop at the Laboratory Computing Resource Center of Argonne National Laboratory. The enthalpy of the redox reaction is computed by subtracting the thermal enthalpy of the overall products from that of the overall reactants [30]. Similarly, any

Scheme 1. The overall redox reactions of Li/TEMPO based NAqHRFB.

unavailable specific heat capacity of a component in the electrolyte is also estimated from DFT calculation. The results are listed in Table S4 in the Supporting Information.

Because of the active thermal management in RFBs, the heat generated inside the stack is mostly dissipated through the tubing and tank walls. It is reasonable to assume that the electrolyte's temperature reaches ambient temperature before it re-enters the stack. Therefore, the stack temperature dictates the thermal stability of electrolyte component materials. To determine whether a HEX is needed, the temperature of the electrolyte flowing out of the stacks is determined using Eq. (11):

$$T_{out} = T_{amb} + \frac{P_r + P_R}{\rho C_p \nu} \tag{11}$$

where $T_{\rm amb}$ is the ambient temperature (298 K), ρ is the density of catholyte, $C_{\rm p}$ is the normalized specific heat capacity of catholyte, and ν is the total flow rate. If $T_{\rm out}$ is higher than the upper temperature limit (60 °C), a HEX will be used to cool the electrolyte down to below the limit. The power required for the cooling HEX is defined in Eq. (12):

$$P_{HEX} = (T_{out} - T_{limit}) \cdot \rho C_p v \tag{12}$$

where $T_{\rm limit}$ is the upper temperature limit. For this manageable thermal model, the heat dissipation of the stacks is ignored, since for RFBs most of the cooling results from the motion of electrolytes. Because of the subtle difference between the specific heat capacities of TEMPO and its charged species TEMPO $^+$, the specific heat capacity of the entire catholyte is considered to be independent of the SOC.

Combining the above TEA model with BPP and HEX models, the capital cost of the system is calculated by dividing the total cost of all components by the nominal energy stored. A series of sensitivity analyses was performed to explore the impact of various conditions, including current density, FEC content, cell voltage, unit price, and equivalent weight of catholyte redoxmers, on the capital cost of NAqHRFB.

Note that the crossover effect is not considered in this initial study. Because of the use of a porous separator, the crossover of redoxmers is inevitable, causing reduced Coulombic efficiency and self-discharge energy loss. Despite this drawback, porous separators have demonstrated decent cyclability for NAqHRFBs [9,11], as can be seen in the flow cell data we used to perform the baseline modeling (Fig. S2). Since lack of reliable selective membranes has been an ongoing challenge for all nonaqueous RFBs, the parasitic materials loss caused by redoxmer crossover through the porous separator is not considered in this initial TEA study.

3. Results and discussion

Using our constructed TEA model, we have obtained the effective discharge voltage $V_{\rm eff}$ from which to calculate the amounts of stack component materials and derive the capital cost. Our baseline case analysis was performed on the Li-graphite/TEMPO system under the reported conditions: electrolyte using 2 M TEMPO in 2.3 M LiPF₆ in EC/PC/EMC (4/1/5 by weight) with 15 wt% FEC, graphite felt electrode (4 mm thick), 800 µm-thick porous separator, flow rate of 50 mL·min $^{-1}$, and current density of $15~{\rm A\cdot m}^{-2}$. These conditions were chosen because they are the state of the art for NAqHRFB tests in high-concentration regimes [9]. In addition, the TEMPO concentration is comparable to mixed-acid vanadium electrolytes in commercial VRFBs, which allows

for direct comparison [15]. Note that the low current density originates from a combination of factors, including slow Li metal deposition or Li⁺ intercalation reactions and high electrolyte viscosity causing severe cell overpotential. The experimental EIS spectrum of this flow cell is plotted in Fig. S2b in the Supporting Information, which is fitted using the included equivalent circuit to obtain a R_{Ω} of 194 Ω cm², a R_{CT} of 28 Ω cm² and a R_{MT} of 2 Ω cm², resulting in a total ASR of 224 Ω cm². With such a concentrated electrolyte, the ohmic resistivity constitutes 87% of the overall ASR and dictates the flow cell performance. This ratio is used approximately in the following catholyte temperature and heat exchanger (HEX) cost modeling, where ohmic resistivity is needed for a specified ASR.

Based on the above conditions, the estimated capital cost turns out to be \$2525 kWh^{-1} and \$10,100 kW^{-1} at the 4 MWh/1 MW scale, which is significantly higher than those of VRFB (\$447 kWh^{-1} and \$4106 kW^{-1}) [24]. As shown by the cost breakdown in Fig. 2, the cell parts, including graphite felt electrode and BPP, are the most cost-intensive components, while the chemical portion (TEMPO, solvents, and salt) is relatively low. Despite the high discharge energy density (\sim 110 Wh·L⁻¹), the power density is relatively low due to the small current density, which entails a large mass of power components and results in the elevated capital cost. The high capital cost represents a formidable barrier to the commercialization of the Li/TEMPO NAqHRFB system. To evaluate its techno-economic potential, it is necessary to analyze its sensitivity to a few selected factors and explore the future space for performance improvement and cost reduction.

Owing to the high power cost, sensitivity to current density was analyzed first. Because of the low ionic conductivity of nonaqueous electrolytes, NAgHRFBs typically exhibit high ASRs, which limits the cells to low-current operation to achieve decent efficiency. With the recent development of nonaqueous RFBs, there is still plenty of space for decreasing ASR and improving current density compared with the above test conditions of Li/TEMPO cells. For example, the use of thinner porous separators (down to 175 µm thick) and graphite felt electrodes (2.5 mm thick) have been demonstrated as viable methods to decrease the ASR to a range of \sim 3–18 Ω cm² in a nonaqueous all-organic RFB, allowing for high operational current densities up to 600 A·m⁻² with an energy efficiency of >65% [31]. Selecting different electrode materials will impact mass and transport behaviors. Compared to graphite felts, woven carbon cloth electrodes with dual-scale pore sizes and low thickness (~400 µm) could provide a large surface area to enable fast transports and low ASRs while maintaining low pressure drop in the cell

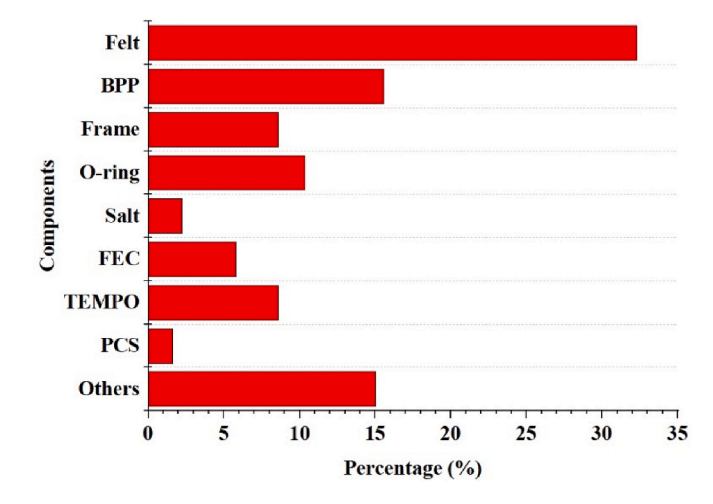


Fig. 2. Breakdown of the calculated baseline capital costs ($$2525 \text{ kWh}^{-1}$$ and $$10,100 \text{ kW}^{-1}$)$ of TEMPO-based NAqHRFB at 4 MWh/1 MW scale. Here, "others" includes separator, endplate, current collector, bolts, HEX, pump, PVC ball valve, solvent, Li metal, pipe, tank, and labor; the cost portion of each is <3%.

[32]. Changing the flow fields from the current flow-through fields to serpentine or interdigitated designs is another possible way to decrease the ASR [33]. These membrane, electrode and flow field engineering strategies could facilitate transport properties and reduce ASR at the catholyte side. However, the Li metal anode side is the limiting factor and allows limited space for increasing current density. Accelerated reaction rates, i.e., increased current densities, will aggravate Li dendrite growth and shorten cycle life. The directly stacked Li strip and graphite felt indeed improve the cyclability of concentrated NAqHRFB cells by transforming Li metal deposition to Li⁺ intercalation reactions without sacrificing cell voltage [11]. High current densities of up to 120 A⋅m⁻² have been successfully demonstrated in Li-graphite/organic flow cells [9,13,34]. However, these reactions involve redox processes in solid phase redoxmers and still suffer from sluggish kinetics compared to the solution phase reaction in the catholyte. These drawbacks are severe technical barriers for high-current operations of NAqHRFB cells, especially in high-concentration regimes. Despite the limitations, exploring the current density-capital cost relationship may shed light on the boundaries and opportunities of NAgHRFBs. Therefore, a sensitivity analysis of the current density was carried out to better understand its effects while assuming the same efficiency.

Following the techniques used for nonaqueous RFBs [31], three different ASR scenarios of 3, 10, and 18 Ω cm² were selected. Sensitivity analyses of current density effects on capital costs in \$ kWh⁻¹ and \$ kW⁻¹ were built, and the results are plotted in Fig. 3a. Interestingly, all cost curves show a dramatic drop as the current density increases from 15 to 150 $\text{A}\cdot\text{m}^{-2}$. A major reason is that at a higher current density the output energy and power of a single cell are enhanced, reducing the number of individual cells needed for achieving the rated energy and power and so decreasing the cost of stack components. However, a further increase in current density does not necessarily result in lower costs. On the one hand, the overpotential (the product of the current density and ASR) simultaneously increases, leading to a lower average discharge voltage (V_{avg}). This is clearly indicated in the computed polarization curves of Li/TEMPO flow cells at the three ASRs in Fig. 3b. The decrease in V_{avg} decreases the energy and power outputs and inverts their cost trend versus current density.

On the other hand, a higher current density will generate more internal heat based on Ohm's law, and this, in addition to the enthalpic heat release, may necessitate a HEX to cool the electrolyte. Heat dissipation is an important design consideration in RFB stacks. Electrolyte

overheating can deteriorate performance and safety, shorten the lifetime, and even cause immediate failure of RFBs. For example, sulfuric acid-based VRFBs need to maintain an operational temperature below 40 °C, because the V⁵⁺ species may undergo parasitic reactions at elevated temperatures, forming solid V₂O₅ precipitations and clogging flow channels [35-39]. Although the circulating electrolytes can offer the advantage of active heat management, in most scenarios this is not sufficient, and passive heat dissipation units such as HEXs are still needed to avoid electrolyte overheating. Similarly, for NAqHRFBs, temperature control is an additional factor that needs to be considered, because overheating can cause safety concerns and have a significant effect on capacity retention. Among all the ingredients in TEMPO-based catholyte, FEC has the lowest thermally stable temperature (60 °C) due to its unstable essence in LiPF₆-based electrolytes, which will generate HF if heated above this temperature [40]. Therefore, we set the upper temperature limit to 60 °C in this work to ensure the thermal stability of the catholyte. This temperature limit could be adjusted if the solution composition changes. Using Eqs. (9)–(11), catholyte temperatures at the stack outlet (T_{out}) were computed using DFT and are plotted in Fig. 3c. The temperature clearly exhibits a rising trend as the current density increases and is elevated to >60 °C at 882 and 659 A·m⁻² for an ASR of 10 and 18 $\Omega \cdot \text{cm}^2$, respectively. With an ASR of 3 $\Omega \cdot \text{cm}^2$, the temperature remains below 60 °C throughout the range of current density under investigation. These are the critical current densities at which HEX operation becomes necessary and the HEX cost starts to be added to the capital cost.

HEX power consumption and cost, as a function of current density at the three ASRs, are plotted in Fig. 3d. These factors show a general trend of flattening and then rising with the increasing current density. It should be noted that ASR has an obvious impact on the capital cost. With a higher ASR (e.g., $18~\Omega~cm^2$), the turning point for the rise appears much earlier with respect to current density, while an ASR of $3~\Omega~cm^2$ leads to delayed flattening of the cost curves even at a current density as high as $750~A·m^{-2}$. As shown in Fig. 3a, for ASRs of 3, 10, and $18~\Omega·cm^2$, the current densities accounting for the minimum costs are 753, 393, and $281~A·m^{-2}$, respectively, which correspond to the energy (power) costs of \$548 kWh⁻¹ (\$2192 kW⁻¹), \$622 kWh⁻¹ (\$2488 kW⁻¹) and \$683 kWh⁻¹ (\$2731 kW⁻¹), respectively. These computed capital costs drop by 78%, 75%, and 73%, respectively, from the initial values, again showing that increasing the operational current density slashes the system cost effectively. Therefore, for a specific measured ASR, the

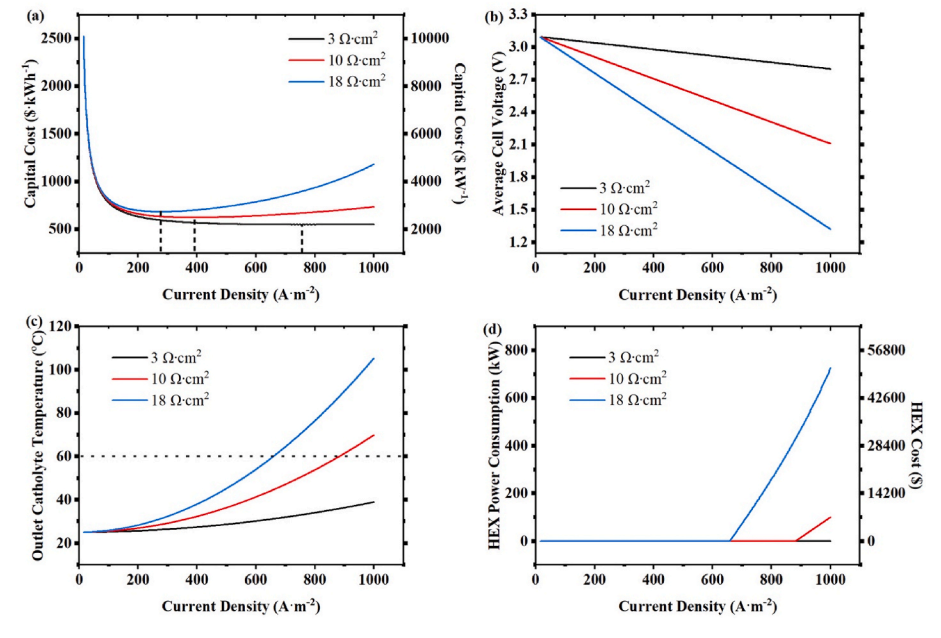


Fig. 3. (a) Sensitivity analysis of capital cost vs. current density. At each ASR, the cost curves in \$kWh⁻¹ and \$kW⁻¹ completely overlap. The dashed lines mark the positions of the lowest capital costs. (b) Computed polarization curves. (c) Computed outlet catholyte temperature as a function of current density. The dashed line indicates the upper temperature limit (60 °C). (d) Computed power consumption and cost of HEX with overlapped curves. Computations were performed at three different ASRs.

current density needs to be optimized within a certain range to achieve the lowest cost. In the best scenario of our Li/TEMPO system, i.e., the one with an ASR of 3 Ω cm², strategies that can manipulate the current density within the range of 200–1000 $A\cdot m^{-2}$, without sacrificing other performance parameters such as cycling efficiency and stability, will be favored in terms of cost.

After the operational effect studies, we next investigated the effects of redoxmer-related materials factors, including unit price, redox potential, and equivalent molecular weight. A variety of catholyte redoxmers with different redox potentials, equivalent molecular weights, and unit prices can be or have been used in NAqHRFBs, such as TEMPO or a derivative of TEMPO (3.5 V) [9], ferrocene (~3.1-3.5 V) [10,11,41], anthraquinone ($2e^-$, ~ 2.4 V) [12], dialkoxylated benzene $(\sim 3.9 \text{ V})$ [13], phenothiazine (1e⁻ or 2e⁻, $\sim 3.6 \text{ V})$ [42,43], and cyclopropenium salts (\sim 4.2–4.5 V) [44,45]. The redox potentials in parentheses are as compared to Li/Li⁺. These candidates may form a new pool for redoxmer selection and expand the space for cost reduction. With the ASR target of 5 Ω cm² in Darling's cost model [18] in mind, we used an ASR value of 3 Ω cm² in the following studies. The current density was set to 200 A·m⁻², instead of the 753 A·m⁻² determined above, based on a combined consideration of capital cost and operational practice. On the one hand, the capital cost at this current density is reasonably close to, only <10% higher than, the minimum value presented above. On the other hand, this current density is considerably close to those reported in realistic NAqHRFBs. For example, up to 120 A·m⁻² were used in organic-based NAqHRFBs, albeit at low redoxmer concentrations (0.1 M) [9,13,34], particularly considering the slow reaction kinetics at the anode side.

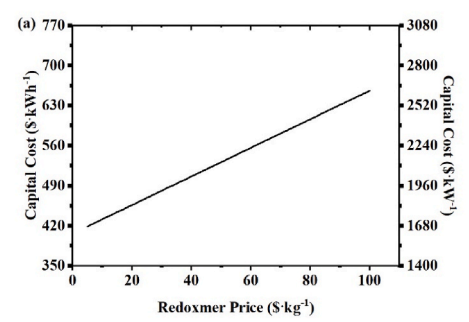
The first materials factor is the unit price of the redoxmer, followed by the prices of other electrolyte components such as solvent and salt. Compared to state-of-the-art VRFBs, the price of TEMPO (\$86 kg⁻¹), much higher than that of V_2O_5 (~\$28 kg⁻¹), remains a concern. Inspired by the above redoxmer candidates and the generally wide structural diversity and tailorability of organic redoxmers, it is possible that less expensive redoxmers with similar properties can be developed and used in NAqHRFBs in the future, so it is of critical importance to explore the effect of redoxmer cost. For this purpose, a sensitivity analysis using unit prices from \$5 kg⁻¹ to \$100 kg⁻¹ was carried out, and the result is plotted in Fig. 4a. Selecting \$5 kg⁻¹ as the lower price limit is based on the redoxmer price target of \$5-\$7 kg⁻¹ in Darling's cost model [18]. Linear relations are shown between the redoxmer price and the capital costs in terms of both kWh-1 and kW-1, indicating the direct consequence of employing cheaper redoxmers. Compared with \$86 kg⁻¹ TEMPO, a $\$5 \text{ kg}^{-1}$ redoxmer decreases energy and power costs by 32%, to $\$419 \text{ kWh}^{-1}$ and $\$1675 \text{ kW}^{-1}$, respectively. These numbers are impressively close to those of VRFB. Therefore, discovering a redoxmer that can be massively produced under moderate conditions to afford a low price is a straightforward approach to the development of cost-effective NAgHRFB systems.

Other major materials used in the electrolyte are significantly less

expensive than TEMPO, such as LiPF₆ (\$20 kg⁻¹), Li metal anode (\$13 kg⁻¹), and organic carbonate solvents (\$1-\$3 kg⁻¹), so their effects on capital cost are not studied here. However, the price of FEC is substantial (\$90 kg⁻¹). In our earlier work, an excessive amount of FEC (15 wt%) was used in high-concentration Li/TEMPO flow cell testing in order to form a stable and compact solid electrolyte interphase (SEI) that leads to extended cycle life [9]. Nevertheless, a lower fraction of FEC, such as 3 wt%, was reported to work effectively in Li metal batteries [46]. This shows that the optimal amount of FEC in Li/TEMPO systems can be investigated to obtain even lower capital costs. A redoxmer unit price of (\$5 kg⁻¹) suggested by the sensitivity analysis in Fig. 4a is used to investigate the effects of the FEC fraction. As shown in Fig. 4b, a linearly declining trend is also observed for the capital cost as the FEC fraction decreases. Reducing the FEC percentage from 15 wt% to 3 wt% cuts the capital cost by 28%, to \$302 kWh⁻¹ and \$1210 kW⁻¹, respectively, indicating its significant effect.

In addition to the unit price, expanding the redoxmer pool also suggests variations in redox potential and equivalent molecular weight. According to Eqs. (6) and (8), a high redox potential, which produces a high cell voltage, will decrease not only the amount of redoxmer but also the number of cells required for achieving the target energy or power, leading to reduced redoxmer and cell part costs. In addition, the redoxmer's equivalent molecular weight per electron involved in the electrochemical reaction is also pertinent to the cost, as the redoxmer price is defined in \$ kg⁻¹. Typically, an equivalent molecular weight below 150 g·mol⁻¹·e⁻¹ is favorable, according to Darling's cost estimate [18]. Therefore, it is of great importance to evaluate the impacts of the redoxmer's potential and equivalent molecular weight on the capital cost. For this purpose, a 2-dimensional sensitivity analysis was performed, with the redox potential ranging from 2 to 4.5 V and the equivalent molecular weight in a range from 50 to 500 g·mol⁻¹·e⁻¹. As shown in Fig. 5, a higher redox potential, a lower equivalent molecular weight, or a combination of both leads to a lower capital cost. This trend was indicated in Eqs. (6) and (8). Because a high value of V_{eff} correlates to a high redox potential and also leads to a smaller number of total cells, both stack parts and redoxmer costs are reduced. In a NAqHRFB scenario with a cell voltage of 4.5 V, an equivalent weight of 150 g·mol⁻¹·e⁻¹, a redoxmer price of 5 kg^{-1} , and a 3 wt% FEC content, the calculated energy cost is 210 kWh^{-1} , which is 53% less than that of VRFB.

To retrospect the impactful parameters on the capital cost of NAqHRFBs, a series of cost breakdowns with the above progressively modified techno-economic parameters are shown in Fig. 6. Interestingly, the progressive sensitivity analyses also show an evolution in the cost contributions of power and energy components. Compared to the baseline case, Scenario A shows a sharp 75% drop in the capital cost at all ASRs as the current density increases from 15 to 200 ${\rm A\cdot m}^{-2}$, indicating it as the most significant cost controller. The cost ratio of power components (graphite felts, separators, BPPs, current collectors, etc.) in the overall capital cost decreases drastically from 77% to 23%, while the energy components (redoxmer, salts, solvents, etc.) become more cost-



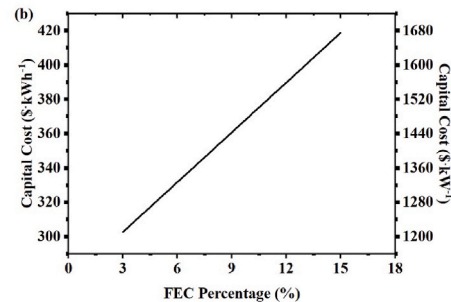


Fig. 4. Sensitivity analyses of (a) redoxmer unit price and (b) FEC fraction on capital cost in kWh⁻¹ and kW⁻¹. Computation conditions: ASR 3 Ω cm² and current density 200 A·m⁻², with a redoxmer price of \$5 kg⁻¹ used in (b); other variables remain the same as Fig. 2.

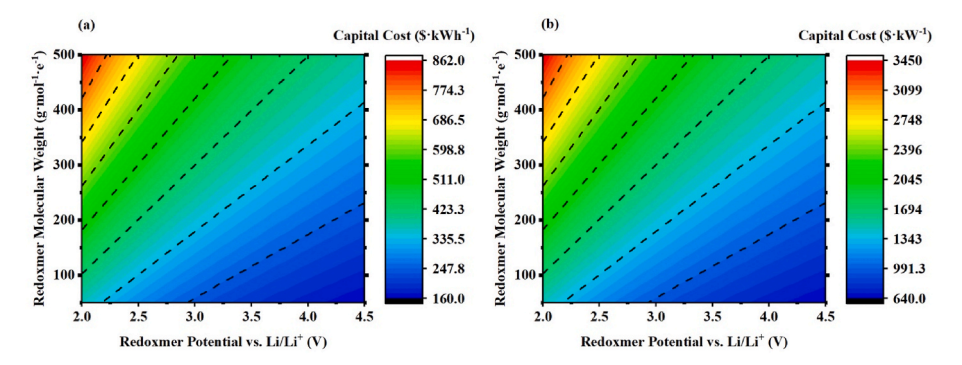


Fig. 5. 2-D sensitivity of the capital costs (indicated by isolines) to cell voltage and redoxmer's equivalent molecular weight. Computation conditions: ASR 3 Ω cm², current density 200 A·m⁻², redoxmer price \$5 kg⁻¹, and FEC content 3 wt%.

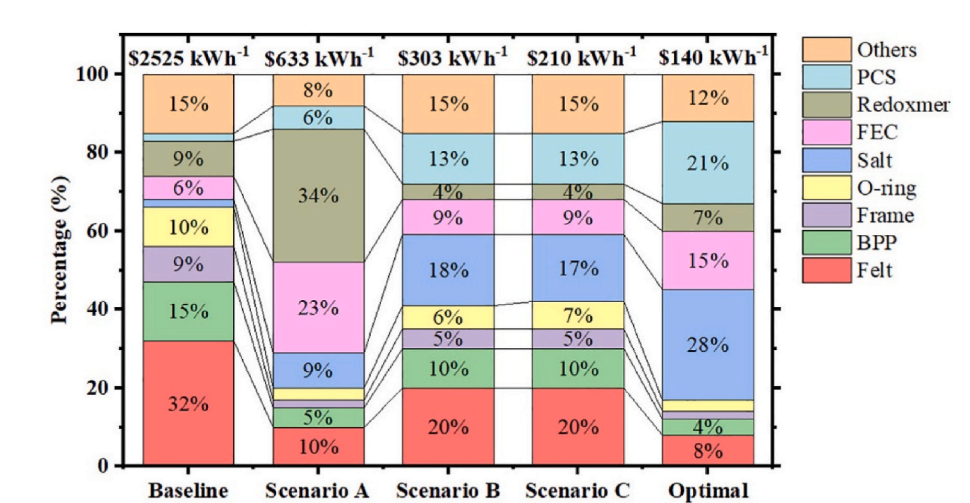


Fig. 6. Cost breakdown for a 4 MWh/1 MW NAqHRFB system, based on five scenarios with progressively modified techno-economic parameters: Baseline (based on the experimental results in Fig. 2), Scenario A (current density 200 A·m $^{-2}$ and ASR 3 Ω cm $^{-2}$), Scenario B (redoxmer price \$5 kg $^{-1}$ and FEC fraction 3 wt%), Scenario C (cell voltage 4.5 V and redoxmer molecular weight 150 g·mol $^{-1}$ ·e $^{-1}$), and Scenario Optimal (current density 753 A·m $^{-2}$). Here, "others" includes separator, endplate, current collector, bolts, HEX, pump, PVC ball valve, solvent, Li metal, pipe, tank, and labor.

intensive, responsible for more than 64% of the overall cost. In Scenario B, the use of inexpensive redoxmers and a decrease in the fraction of expensive electrolyte compositions further cuts the capital cost by more than 50%, and it is quite clear that the cost reduction falls more heavily on the energy components. Elevating the redox potential and pruning the equivalent molecular weight of redoxmer to target values, as in Scenario C, lead to a one third reduction in capital cost, but with almost unchanged cost distributions. Finally, the optimal current density 753 A·m⁻² obtained from the previous current density sensitivity analysis is used to calculate the capital cost in an ideal scenario. The energy cost is further reduced to \$140 kWh⁻¹, which is impressively lower than DOE's long-term goal of \$150 kWh⁻¹ for stationary storage. In this scenario, it is readily observed that the power components contribute only 20% to the total cost, and the highest contributor to cost is the energy components. Although the high current density might be operationally challenging for NAqHRFBs, the significantly low energy and power costs suggest that NAqHRFBs can be an attractive cost-effective storage solution.

These sensitivity analyses show that, to realize the computed cost prospect of NAqHRFBs, the most critical need is to overcome the barriers to achieving high operational current densities in NAqHRFBs that use inexpensive redoxmers at a high concentration. Although challenging, this future research objective requires urgent attention. As a predictive TEA model, other practical issues associated with safety, operating atmosphere, and cycle life are not considered here, but these are also essential challenges that need to be addressed to make NAqHRFBs feasible at large scales.

4. Conclusion

In summary, a TEA model has been established to compute the capital cost for NAqHRFB systems at relevant scales of storage. This model encompasses a number of key operational and materials parameters to identify determining factors and suggests research needs to overcome the current limitations for NAqHRFBs. Starting with the effective discharge voltage V_{eff} , the pump loss, and heat exchange, we obtained the amounts and costs of electrolyte and stack part materials needed to achieve the target energy and power to derive the capital costs. In a series of progressive sensitivity analyses, the key costintensive factors have been determined, including the operational current density, redoxmer price, and FEC content. Improving these systemlevel operational and materials metrics, such as increasing the current density by a factor of 10, decreasing the redoxmer price by a twentieth, or reducing the FEC content by 80% compared to the current state of the art, has been demonstrated effective to produce cost-competitive NAqHRFBs. The results also suggest potential future research directions to break through these major cost and performance roadblocks. Under virtually optimized conditions, NAqHRFBs can have energy costs lower than that of VRFBs and even below DOE's cost target for stationary storage, suggesting their latent characteristics as cost-effective storage solutions. Note that the NAqHRFB system studied here is for a 4-h storage and the cost would be even lower for longer durations.

This model developed here is an effective tool for determining the techno-economic performance of NAqHRFBs based on selected experimental and materials parameters. While this model is not without limitations, such as the omission of the shunt current and the lack of levelized cost modeling (an indicator for operational cost), those can be

addressed when long-term cycling performance under the identified conditions is available. The universal framework of this model makes it a tool generally suited for capital cost analysis. With more data regarding material production cost and performance under standardized conditions becoming available, this framework can evolve to provide more comprehensive analysis of various RFB systems.

Note

The authors declare no conflict of interest.

CRediT authorship contribution statement

Zhiguang Li: Methodology, Investigation, Modeling, Writing – original draft. Xiaoting Fang: Methodology, Investigation. Lei Cheng: Supervision. Xiaoliang Wei: Conceptualization, Methodology, Writing – review & editing. Lu Zhang: Conceptualization, Methodology, Writing – review & editing.

Declaration of competing interest

The authors declare that they have no known competing financial interests or personal relationships that could have appeared to influence the work reported in this paper.

Acknowledgement

This research was financially supported by Laboratory Directed Research and Development (LDRD) funding from Argonne National Laboratory, provided by the Director, Office of Science, of the U.S. Department of Energy under Contract No. DE-AC02-06CH11357. The submitted manuscript has been created by UChicago Argonne, LLC, Operator of Argonne National Laboratory ("Argonne"). Argonne, a U.S. Department of Energy Office of Science laboratory, is operated under Contract No. DE-AC02-06CH11357. This work is also supported by the Joint Center for Energy Storage Research (JCESR), an Energy Innovation Hub funded by the U.S. Department of Energy, Office of Science, and Basic Energy Sciences and National Science Foundation (Award No. CHE-2055222). The authors thank Dr. Shabbir Ahmed for inspiring discussions.

Appendix A. Supplementary data

Supplementary data to this article can be found online at https://doi.org/10.1016/j.jpowsour.2022.231493.

References

- [1] K. Kusakana, Optimization of the daily operation of a hydrokinetic-diesel hybrid system with pumped hydro storage, Energy Convers. Manag. 106 (2015) 901–910, https://doi.org/10.1016/j.enconman.2015.10.021.
- [2] G.L. Soloveichik, Flow batteries: current status and trends, Chem. Rev. 115 (20) (2015) 11533–11558, https://doi.org/10.1021/cr500720t.
- [3] On Location, Electricity storage technology review. https://www.energy.gov/site s/default/files/2020/10/f79/Electricity%20Storage%20Technologies%20%20Re port.pdf, 2020.
- [4] J. Winsberg, T. Hagemann, T. Janoschka, M.D. Hager, U.S. Schubert, Redox-flow batteries: from metals to organic redox-active materials, Angew. Chem. Int. Ed. 56 (2017) 686–711, https://doi.org/10.1002/anie.201604925.
- [5] C. Minke, T. Hickmann, A.R. dos Santos, U. Kunz, T. Turek, Cost and performance prospects for composite bipolar plates in fuel cells and redox flow batteries, J. Power Sources 305 (2016) 182–190, https://doi.org/10.1016/j. ipowsour.2015.11.052.
- [6] U.S. Department of Energy Office of Electricity Delivery and Energy Reliability, Energy storage program planning document. https://www.energy.gov/sites/d efault/files/oeprod/DocumentsandMedia/OE_Energy_Storage_Program_Plan_ Feburary 2011v3.pdf, 2011.
- [7] S.H. Shin, S.H. Yun, S.H. Moon, A review of current developments in non-aqueous redox flow batteries: characterization of their membranes for design perspective, RSC Adv. 3 (24) (2013) 9095–9116, https://doi.org/10.1039/c3ra00115f.

- [8] K. Gong, Q.R. Fang, S. Gu, S.F.Y. Li, Y.S. Yan, Nonaqueous redox-flow batteries: organic solvents, supporting electrolytes, and redox pairs, Energy Environ. Sci. 8 (12) (2015) 3515–3530, https://doi.org/10.1039/c5ee02341f.
- [9] X. Wei, W. Xu, M. Vijayakumar, L. Cosimbescu, T. Liu, V. Sprenkle, W. Wang, TEMPO-based catholyte for high-energy density nonaqueous redox flow batteries, Adv. Mater. 26 (45) (2014) 7649–7653, https://doi.org/10.1002/ adma.201403746.
- [10] Y. Zhao, Y. Ding, J. Song, G. Li, G.B. Dong, J.B. Goodenough, G.H. Yu, Sustainable electrical energy storage through the ferrocene/ferrocenium redox reaction in aprotic electrolyte, Angew. Chem. Int. Ed. 53 (41) (2014) 11036–11040, https://doi.org/10.1002/anie.201406135.
- [11] X.L. Wei, L. Cosimbescu, W. Xu, J.Z. Hu, M. Vijayakumar, J. Feng, M.Y. Hu, et al., Towards high-performance nonaqueous redox flow electrolyte via ionic modification of active species, Adv. Energy Mater. 5 (1) (2015), 1400678, https://doi.org/10.1002/aenm.201400678.
- [12] W. Wang, W. Xu, L. Cosimbescu, D.W. Choi, L.Y. Li, Z.G. Yang, Anthraquinone with tailored structure for a nonaqueous metal-organic redox flow battery, Chem. Commun. 48 (53) (2012) 6669–6671, https://doi.org/10.1039/C2cc32466k.
- [13] J. Zhang, Z. Yang, I.A. Shkrob, R.S. Assary, S.O. Tung, B. Silcox, W. Duan, et al., Annulated dialkoxybenzenes as catholyte materials for nonaqueous redox flow batteries: achieving high chemical stability through bicyclic substitution, Adv. Energy Mater. 7 (2017), 1701272, https://doi.org/10.1002/aenm.201701272.
- [14] H.L. Pan, X.L. Wei, W.A. Henderson, Y.Y. Shao, J.Z. Chen, P. Bhattacharya, J. Xiao, J. Liu, On the way toward understanding solution chemistry of lithium polysulfides for high energy Li-S redox flow batteries, Adv. Energy Mater. 5 (16) (2015), 1500113, https://doi.org/10.1002/aenm.201500113.
- [15] L.Y. Li, S. Kim, W. Wang, M. Vijayakumar, Z.M. Nie, B.W. Chen, J.L. Zhang, et al., A stable vanadium redox-flow battery with high energy density for large-scale energy storage, Adv. Energy Mater. 1 (3) (2011) 394–400, https://doi.org/ 10.1002/aenm.201100008.
- [16] X. Zhang, Y. Yang, Z. Zhou, Towards practical lithium-metal anodes, Chem. Soc. Rev. 49 (10) (2020) 3040–3071, https://doi.org/10.1039/C9CS00838A.
- [17] J.-G. Zhang, W. Xu, J. Xiao, X. Cao, J. Liu, Lithium metal anodes with nonaqueous electrolytes, Chem. Rev. 120 (24) (2020) 13312–13348, https://doi.org/10.1021/ acs.chemrev.0c00275.
- [18] R.M. Darling, K.G. Gallagher, J.A. Kowalski, S. Ha, F.R. Brushett, Pathways to low-cost electrochemical energy storage: a comparison of aqueous and nonaqueous flow batteries, Energy Environ. Sci. 7 (11) (2014) 3459–3477, https://doi.org/10.1039/c4ee02158d.
- [19] J. Noack, L. Wietschel, N. Roznyatovskaya, K. Pinkwart, J. Tübke, Technoeconomic modeling and analysis of redox flow battery systems, Energies 9 (8) (2016) 627, https://doi.org/10.3390/en9080627.
- [20] A. Crawford, V. Viswanathan, D. Stephenson, W. Wang, E. Thomsen, D. Reed, B. Li, P. Balducci, M. Kintner-Meyer, V. Sprenkle, Comparative analysis for various redox flow batteries chemistries using a cost performance model, J. Power Sources 293 (2015) 388–399, https://doi.org/10.1016/j.jpowsour.2015.05.066.
- [21] V. Dieterich, J.D. Milshtein, J.L. Barton, T.J. Carney, R.M. Darling, F.R. Brushett, Estimating the cost of organic battery active materials: a case study on anthraquinone disulfonic acid, Transl. Mater. Res. 5 (2018), 034001, https://doi. org/10.1088/2053-1613/aach0e
- [22] S.M. Laramie, J.D. Milshtein, T.M. Breault, F.R. Brushett, L.T. Thompson, Performance and cost characteristics of multi-electron transfer, common ion exchange non-aqueous redox flow batteries, J. Power Sources 327 (2016) 681–692, https://doi.org/10.1016/j.jpowsour.2016.07.015.
- [23] Shuhei Maeda, Jun Sugawara, Hiroshi Hayami, Bipolar Plate for Redox Flow Battery, 2013. PCT/JP2011/058524 filed Apr. 4, 2011. Patent Application No. US 2013/0037760 A1, published Feb. 14, 2013.
- [24] V. Viswanathan, A. Crawford, D. Stephenson, S. Kim, W. Wang, B. Li, G. Coffey, et al., Cost and performance model for redox flow batteries, J. Power Sources 247 (2014) 1040–1051, https://doi.org/10.1016/j.jpowsour.2012.12.023.
- [25] X.L. Wei, W. Xu, J.H. Huang, L. Zhang, E. Walter, C. Lawrence, M. Vijayakumar, et al., Radical compatibility with nonaqueous electrolytes and its impact on an allorganic redox flow battery, Angew. Chem. Int. Ed. 54 (30) (2015) 8684–8687, https://doi.org/10.1002/anje.201501443.
- [26] S. Whitaker, Flow in porous media I: a theoretical derivation of Darcy's law, Transport Porous Media 1 (1986) 3–25, https://doi.org/10.1007/BF01036523
- [27] R.G. Parr, On the genesis of a theory, Int. J. Quant. Chem. 37 (1990) 327–347, https://doi.org/10.1002/QUA.560370407.
- [28] P. Hohenberg, W. Kohn, Inhomogeneous electron gas, Phys. Rev. 136 (3B) (1964) B864–B871, https://doi.org/10.1103/PhysRev.136.B864.
- [29] D.R. Hartree, The wave mechanics of an atom with a non-coulomb central field. Part II. Some results and discussion, Math. Proc. Camb. Phil. Soc. 24 (1) (1928) 111–132, https://doi.org/10.1017/S0305004100011920.
- [30] J.W. Ochterski, Thermochemistry in Gaussian, 2002. Gaussian.com, https://gaussian.com/wp-content/uploads/dl/thermo.pdf.
- [31] X. Wei, W. Duan, J. Huang, L. Zhang, B. Li, D. Reed, W. Xu, V. Sprenkle, W. Wang, A high-current, stable nonaqueous organic redox flow battery, ACS Energy Lett. 1 (4) (2016) 705–711, https://doi.org/10.1021/acsenergylett.6b00255.
- [32] A. Forner-Cuenca, E.E. Penn, A.M. Oliveira, F.R. Brushett, Exploring the role of electrode microstructure on the performance of non-aqueous redox flow batteries, J. Electrochem. Soc. 166 (10) (2019) A2230–A2241, https://doi.org/10.1149/ 2.0611910jes.
- [33] X. Ke, J.M. Prahl, J.I.D. Alexander, J.S. Wainright, T.A. Zawodzinski, R.F. Savinell, Rechargeable redox flow batteries: flow fields, stacks and design considerations, Chem. Soc. Rev. 47 (23) (2018) 8721–8743, https://doi.org/10.1039/c8cs00072g.

- [34] Y. Zhao, J. Zhang, G. Agarwal, Z. Yu, R.E. Corman, Y. Wang, L.A. Robertson, et al., TEMPO allegro: liquid catholyte redoxmers for nonaqueous redox flow batteries, J. Mater. Chem. 9 (2021) 16769–16775, https://doi.org/10.1039/dlta04297a.
- [35] M. Kazacos, M. Cheng, M. Skyllas-Kazacos, Vanadium redox cell electrolyte optimization studies, J. Appl. Electrochem. 20 (1990) 463–467, https://doi.org/ 10.1007/BF01076057.
- [36] K. Wang, Y. Zhang, L. Liu, J. Xi, Z. Wu, X. Qiu, Broad temperature adaptability of vanadium redox flow battery-Part 3: the effects of total vanadium concentration and sulfuric acid concentration, Electrochim. Acta 259 (2018) 11–19, https://doi. org/10.1016/j.electacta.2017.10.148.
- [37] M. Skyllas-Kazacos, L. Cao, M. Kazacos, N. Kausar, A. Mousa, Vanadium electrolyte studies for the vanadium redox battery—a review, ChemSusChem 9 (13) (2016) 1521–1543, https://doi.org/10.1002/cssc.201600102.
- [38] D. Oboroceanu, N. Quill, C. Lenihan, D.N. Eidhin, S.P. Albu, R.P. Lynch, D. N. Buckley, Effects of temperature and composition on catholyte stability in vanadium flow batteries: measurement and modeling, J. Electrochem. Soc. 164 (9) (2017) A2101–A2109, https://doi.org/10.1149/2.1401709jes.
- [39] M. Skyllas-Kazacos, C. Menictas, M. Kazacos, Thermal stability of concentrated V (V) electrolytes in the vanadium redox cell, ChemInform 27 (1996), https://doi. org/10.1002/CHIN.199633008.
- [40] K. Kim, I. Park, S.-Y. Ha, Y. Kim, M.-H. Woo, M.-H. Jeong, W.C. Shin, M. Ue, S. Y. Hong, N.-S. Choi, Understanding the thermal instability of fluoroethylene

- carbonate in LiPF 6 -based electrolytes for lithium ion batteries, Electrochim. Acta 225 (2017) 358–368, https://doi.org/10.1016/j.electacta.2016.12.126.
- [41] G.T. Cong, Y.C. Zhou, Z.J. Li, Y.C. Lu, A highly concentrated catholyte enabled by a low-melting-point ferrocene derivative, ACS Energy Lett. 2 (4) (2017) 869–875, https://doi.org/10.1021/acsenergylett.7b00115.
- [42] J.D. Milshtein, A.P. Kaur, M.D. Casselman, J.A. Kowalski, S. Modekrutti, P. L. Zhang, N.H. Attanayake, et al., High current density, long duration cycling of soluble organic active species for non-aqueous redox flow batteries, Energy Environ. Sci. 9 (11) (2016) 3531–3543, https://doi.org/10.1039/c6ee02027e.
- [43] N.H. Attanayake, J.A. Kowalski, K.V. Greco, M.D. Casselman, J.D. Milshtein, S. J. Chapman, S.R. Parkin, F.R. Brushett, S.A. Odom, Tailoring two-electron-donating phenothiazines to enable high-concentration redox electrolytes for use in nonaqueous redox flow batteries, Chem. Mater. 31 (12) (2019) 4353–4363.
- [44] C.S. Sevov, S.K. Samaroo, M.S. Sanford, Cyclopropenium salts as cyclable, high-potential catholytes in nonaqueous media, Adv. Energy Mater. 7 (5) (2017), 1602027, https://doi.org/10.1002/aenm.201602027.
- [45] Y. Yan, S.G. Robinson, M.S. Sigman, M.S. Sanford, Mechanism-based design of a high-potential catholyte enables a 3.2 V all-organic nonaqueous redox flow battery, J. Am. Chem. Soc. 141 (38) (2019) 15301–15306, https://doi.org/ 10.1021/jacs.9b07345.
- [46] X.-Q. Zhang, X.-B. Cheng, X. Chen, C. Yan, Q. Zhang, Fluoroethylene carbonate additives to render uniform Li deposits in lithium metal batteries, Adv. Funct. Mater. 27 (10) (2017), 1605989, https://doi.org/10.1002/adfm.201605989.